

1 **First-principles study on atomic configuration of electron-beam**  
2 **irradiated C<sub>60</sub> clusters**

3 Tomoya Ono

4 *Graduate School of Engineering, Osaka University, Suita, Osaka 565-0871, Japan*

5 Shigeru Tsukamoto

6 *Peter Grünberg Institut & Institute for Advanced Simulation,*  
7 *Forschungszentrum Jülich and JARA, D-52425 Jülich, Germany*

8 (Dated: November 9, 2018)

### Abstract

A theoretical study proposes the atomic configuration of electron-beam irradiated C<sub>60</sub> thin films. We examined the electronic structure and electron-transport properties of the C<sub>60</sub> clusters using density-functional calculations and found that a rhombohedral C<sub>60</sub> polymer with  $sp^3$ -bonded dumbbell-shaped connections at the molecule junction is a semiconductor with a narrow band gap while the polymer changes to exhibit metallic behavior by forming  $sp^2$ -bonded peanut-shaped connections. Conductance below the Fermi level increases and the peak of the conductance spectrum arising from the  $t_{u1}$  states of a C<sub>60</sub> molecule becomes obscure after the connections are rearranged. The present rhombohedral film, including the [2+2] four-membered rings and peanut-shaped connections, is a candidate to represent the structure of the metallic C<sub>60</sub> polymer at the initial stage of electron-beam irradiation.

9 PACS numbers: 71.30.+h, 71.15.Mb, 72.80.Rj, 73.61.Wp

## 10 I. INTRODUCTION

11 Intermolecular electron transport has attracted a great deal of attention in numerous fields  
12 of research accompanied by the progress in nanostructure-fabrication technology. Fullerene-  
13 based molecular crystals and films are of particular interest because of their very rich physical  
14 properties such as superconductivity and magnetism. The polymerization of  $C_{60}$  molecules  
15 in the solid phase using various techniques, e.g., photoirradiation or electron-beam (EB)  
16 irradiation, have resulted in new forms of carbon materials.<sup>1</sup> The first-principles study by  
17 Okada and Oshiyama reported that the band gap of the rhombohedral phase of the  $C_{60}$   
18 polymer linked by [2+2] four-membered rings, where two C atoms shared by the two adjacent  
19 hexagons in a  $C_{60}$  molecule are covalently bonded to the C atoms shared by the two hexagons  
20 in the neighboring  $C_{60}$  molecule (e.g., see Fig. 1), is significantly smaller than that of  $C_{60}$   
21 bulk.<sup>2</sup> Onoe *et al.* found that  $C_{60}$  films change to polymers accompanying the insulator-  
22 metal transition due to EB irradiation and that a one-dimensional (1D) peanut-shaped  
23 connection is formed, where  $C_{60}$  molecules are linked by  $sp^2$ -like connections instead of  
24  $sp^3$ -like connections,<sup>3</sup> and intensive studies on electron transport in the  $C_{60}$  polymer have  
25 been carried out up to now.<sup>4</sup> First-principles calculations on the electronic structure of  
26 three-dimensional (3D)  $C_{60}$  polymers have revealed that 1D peanut-shaped  $C_{60}$  polymers  
27 are insulators and electrons are conducted across the 1D polymers via [2+2] four-membered  
28 rings between the two peanut-shaped  $C_{60}$  polymers in the 3D hexagonal structure,<sup>5,6</sup> which  
29 is a completely different configuration from the face-centered cubic structure of  $C_{60}$  bulk.

30 Nakaya *et al.* recently revealed that the chemical linkage between  $C_{60}$  molecules created  
31 by EB irradiation are thermally more stable than the [2+2] four-membered ring because the  
32 polymers are stable under thermal annealing at 220 °C, which is higher than the decomposi-  
33 tion temperature of the [2+2] four-membered rings, and they claimed that a peanut-shaped  
34 fullerene contributes to the metallic characteristics of EB irradiated film.<sup>7</sup> They also demon-  
35 strated by scanning-tunneling spectroscopy (STS) that the characteristic peak of spectra  
36 of the  $C_{60}$  molecule disappears at its polymerized center after EB irradiation. Moreover,  
37 their scanning tunneling microscopy (STM) images demonstrated that the  $C_{60}$  polymers  
38 retain a *rhombohedral* structure at the initial stage of EB irradiation; however, this result  
39 does not agree with the *hexagonal* structure derived by Onoe *et al.* using first-principles  
40 calculations.<sup>5,6</sup> Thus, the physics underlying the generation of conductivity in EB irradiated

41  $C_{60}$  films remains unclear.

42 In this paper, the atomic configuration of the EB irradiated  $C_{60}$  film is proposed by using  
43 first-principles calculations. We examine what effect the bond configuration at the molecule  
44 junctions has on the electronic structure and electron-transport properties to interpret the  
45 generation of conductivity in EB irradiated  $C_{60}$  films. Our findings are that the rhombo-  
46 hedral  $C_{60}$  polymer consisting of the [2+2] four-membered rings and the  $sp^3$ -like interlayer  
47 connections create a semiconductor with a narrow band gap and the band gap vanishes  
48 when the  $sp^2$ -like interlayer connection is formed. We found significant differences between  
49 the conduction spectra of the dimers bonded by the  $sp^3$ -like and  $sp^2$ -like connections; the  
50 conductance of the  $sp^2$ -like bonded dimer was higher than that of the  $sp^3$ -like bonded dimer  
51 below the Fermi level and the peak of the conductance spectrum caused by the  $t_{u1}$  orbitals  
52 of the  $sp^3$ -like bonded dimer was clear while that of the  $sp^2$ -like bonded dimer was obscure.

53 All calculations are performed within the framework of density functional theory<sup>8</sup> using  
54 the real-space finite-difference approach, which enables us to determine the self-consistent  
55 electronic ground state with a high degree of accuracy by using a timesaving double-grid  
56 technique.<sup>9,10</sup> The norm-conserving pseudopotentials<sup>11</sup> of Troullier and Martins<sup>12</sup> are used  
57 to describe electron-ion interaction, and exchange correlation effects are treated with local  
58 density approximation.<sup>13</sup>

## 59 II. ELECTRONIC STRUCTURE OF $C_{60}$ POLYMERS

60  $C_{60}$  polymers form a triangular lattice with [2+2] four-membered rings in each poly-  
61 merized layer and the layers are stacked along a direction perpendicular to the layers in  
62 a rhombohedral symmetry.<sup>2</sup> When the *ABC*-stacking structure<sup>14</sup> is formed, the layers are  
63 bonded by  $sp^3$ -like connections, in which the hexagons on neighboring  $C_{60}$  molecules are  
64 brought face to face. When the C-C bonds sheared by a hexagon and pentagon on the  
65 facing hexagons are distorted, the layers are linked by an  $sp^2$ -like connection consisting  
66 of hexagons and heptagons. After this, we will refer to  $sp^3$ -like interlayer connections as  
67 dumbbell-shaped and  $sp^2$ -like interlayer connection as peanut-shaped. The peanut-shaped  
68 connection is much stronger than the [2+2] four-membered ring because the energy to form  
69 it is smaller than that for the [2+2] four-membered ring by 0.02 eV/atom.<sup>15</sup> Therefore, the  
70 polymer can be reinforced by the peanut-shaped connection so that it can survive under

71 thermal annealing. We first calculate the electronic structure of the  $C_{60}$  polymers.

72 Figure 1 shows two geometries of the models studied here. The  $C_{60}$  polymers in model (a)  
73 are bonded by the [2+2] four-membered rings in the layer and linked by the dumbbell-shaped  
74 connections between the layers. In model (b), one of the dumbbell-shaped connections  
75 between the layers is deformed into the peanut-shaped connection. Since the metallic phase  
76 of the  $C_{60}$  polymer is surrounded by the other phase of the  $C_{60}$ s at the initial stage of  
77 the EB irradiation according to the STM image,<sup>7</sup> its lattice parameters are not expected  
78 to be fully relaxed. We assume lattice parameters  $a=17.37$  bohr,  $c=46.30$  bohr and  $\alpha =$   
79  $\pi/3$ , which correspond to those for the dumbbell-shaped interlayer connection obtained  
80 by the x-ray diffraction pattern analysis,<sup>16</sup> and employ these lattice parameters for both  
81 model (a) and model (b) to compare the contribution of the dumbbell-shaped and peanut-  
82 shaped connections to the electronic structures. Note that the stacking structure of the  
83 polymer presented in this study is not deformed from the rhombohedral bulk phase and  
84 corresponds to the experimentally observed STM image whereas the hexagonal polymers in  
85 Refs. 5 and 6 require drastic structural deformation. Integration in the Brillouin zone is  
86 carried out using 24-point sampling and structural optimization for the atomic geometris  
87 is implemented for both models until the remaining forces for each atom are less than 36  
88 meV/bohr. The calculated electronic band structures are depicted in Fig. 2. The energy  
89 band gap is reduced by forming peanut-shaped connections; the peanut-shaped polymer  
90 exhibits metallic behavior while model (a) is a semiconductor with a fundamental band gap  
91 of  $\sim 0.6$  eV. The formation energy of model (b) is larger than that of model (a) by 0.25  
92 eV/atom although the formation energy of an isolated peanut-shaped dimer is smaller than  
93 that of a dumbbell-shaped dimer by 0.04 eV/atom. Thus, the peanut-shaped connections are  
94 not widely generated but  $C_{60}$  molecules form small clusters with peanut-shaped connections  
95 in the film after EB irradiation.

### 96 III. TRANSPORT PROPERTIES OF $C_{60}$ DIMERS

97 The STS spectra, which have been employed to interpret the transport properties of  
98 molecules, show peaks which are distinctly associated with the electronic structure of  
99 molecules.<sup>17</sup> However, to replicate the STS spectrum of the  $C_{60}$  cluster in the  $C_{60}$  film, the  
100 system including the large number of atoms are required because a  $C_{60}$  molecule contains

101 60 atoms, which is not easy task by the present computational resources. Moreover, the  
 102 number of peaks measured for the considered bias-voltage range have been smaller than  
 103 the number of electronic states in the molecules within the corresponding energy window in  
 104 some cases.<sup>18</sup> This fact implies that some states of molecules do not contribute to electron  
 105 transport and that a simple interpretation of transport properties only in terms of DOS  
 106 is insufficient. In addition, it is well known that the junction between C<sub>60</sub> molecules are  
 107 a bottleneck for electron transport<sup>19–21</sup> and the energy gap between the highest-occupied  
 108 molecular orbital (HOMO) and the lowest-unoccupied molecular orbital (LUMO) decreases  
 109 after polymerization.<sup>5,6,15,22</sup> One of the present authors (S.T.) examined variations in the  
 110 local density of states (LDOS) along the 1D C<sub>60</sub> polymer axis and demonstrated that the  
 111 energy gap of LDOS at the molecule junction is larger than that in the C<sub>60</sub> molecules.<sup>15</sup>  
 112 The *sp*<sup>2</sup>-like connections of the peanut-shaped polymer might enhance electron transport  
 113 because  $\pi$  electrons are major carriers in metallic carbon nanotubes. Thus, it is of con-  
 114 siderable interest to examine how the difference in the bond network between fullerenes  
 115 contributes to electron transport through fullerenes.

116 We explore the contribution of the peanut-shaped connection to electron-transport prop-  
 117 erties. Figure 3 shows the computational model, where a C<sub>60</sub> dimer is sandwiched between  
 118 electrodes. Since the lattice-constant mismatch between the C<sub>60</sub> polymers and the elec-  
 119 trodes gives rise to further complex discussions on the transport properties, we employ the  
 120 simplified models to focus on the difference in the contributions to the transport properties  
 121 between the dumbbell-shaped and peanut-shaped connections. To determine the optimized  
 122 atomic coordinates and Kohn-Sham effective potential, we use a conventional supercell un-  
 123 der a periodic boundary condition in all directions with a real-space grid spacing of  $\sim 0.32$   
 124 bohr; the dimensions of the supercell are  $L_x = 37.87$  bohr,  $L_y = 37.49$  bohr, and  $L_z = 71.15$   
 125 bohr, where  $L_x$  and  $L_y$  are the lateral lengths of the supercell in the  $x$ - and  $y$ -directions  
 126 parallel to the electrode surfaces, respectively, and  $L_z$  is the length in the  $z$  direction.  
 127 Structural optimizations are implemented in advance for the isolated peanut-shaped dimer  
 128 and it is then placed between the electrodes, where the three topmost surface atomic lay-  
 129 ers are atomistic Al(111) and the rest are aluminum jellium. The dimer is aligned at the  
 130 hexagonal-close-packed-hollow site on the (111) surface facing a hexagon, which is the most  
 131 stable configuration for a C<sub>60</sub> molecule on a face centered cubic (111) surface according to  
 132 first-principles calculations.<sup>23</sup> The distance between the surface atomic layers on the left

133 and right electrodes is set at 35.81 bohr so that the distance between the edge atoms of the  
134 dimer and the surface atomic layer of the electrodes corresponds to that reported by first-  
135 principles calculations. The dimer is relaxed between the electrodes. The atomic geometries  
136 of 36 carbon atoms for the dumbbell-shaped dimer at the molecule junction are modified  
137 from the above mentioned structure and structural optimization is also implemented.

138 We take a grid spacing of  $\sim 0.47$  a.u for the electron-transport calculations. We ensured  
139 that the decreased grid spacing and the enlarged supercell would not significantly affect our  
140 results. The scattering wave functions of the electrons propagating from the electrodes are  
141 determined by using the method of overbridging boundary matching.<sup>24-26</sup> The retarded self-  
142 energy matrices for aluminum jellium are employed to include the rest of the semi-infinite  
143 electrodes. Since the DOS of aluminum is similar to that of free electrons, unfavorable  
144 effects from the DOS of the electrodes on the conductance spectra can be eliminated. We  
145 first calculate the Kohn-Sham effective potential using the supercell employed in structural  
146 optimization and then compute the scattering wave functions obtained non-self-consistently.  
147 It has been reported that this procedure is just as accurate in the linear response regime but  
148 significantly more efficient than performing computations self-consistently on a scattering-  
149 wave basis.<sup>27</sup> The conductance of the dimers is described by the Landauer-Büttiker formula,  
150  $G = \text{Tr}(\mathbf{T}^\dagger \mathbf{T})G_0$ ,<sup>28</sup> where  $\mathbf{T}$  is a transmission-coefficient matrix.

151 Figure 4 plots the conductance spectra of the dumbbell-shaped and peanut-shaped dimers  
152 as a function of the energy of incident electrons. The magnitude of conductance at the Fermi  
153 level and the conduction spectra as a function of the energy of the incident electrons for  
154 the dumbbell-shaped dimer are in agreement with those reported in another theoretical  
155 study.<sup>21</sup> Since the dimers are not connected by the [2+2] four-membered rings in a direction  
156 parallel to the electrode and the 1D  $C_{60}$  polymers act as an insulator, the conductance  
157 of the dimers is low around the Fermi level. This implies that the [2+2] four-membered  
158 rings play an important role in the metallic characteristics of the  $C_{60}$  polymers and the  
159 very bright  $C_{60}$  molecule in the experimental STM image<sup>7</sup> is presumably linked by the  
160 [2+2] four-membered rings and the peanut-shaped connections as explained in the preceding  
161 section. The difference in energy between the peaks of the spectrum around the Fermi level  
162 corresponds to the energy gap between the HOMO and the LUMO of the isolated dimers.  
163 The peak at  $E_F + 0.25$  eV is attributed to the triply degenerate LUMO ( $t_{u1}$ ) of a  $C_{60}$   
164 molecule, where  $E_F$  is the Fermi level. The conductance of the peanut-shaped dimer is

165 higher than that of the dumbbell-shaped dimer below the Fermi level and the peak of the  
 166 conductance spectrum induced by the  $t_{u1}$  orbitals of the dumbbell-shaped dimer is clearer  
 167 than that of the peanut-shaped dimer.

168 To examine the contribution of the peanut-shaped connection to the electron-transport  
 169 properties in more detail, Fig. 5 shows the LDOS of the dimers, which have been plotted by  
 170 integrating them along the plane parallel to the electrode surface,  $\rho(z, E) = \int |\psi(\mathbf{r}, E)|^2 d\mathbf{r}_{\parallel}$ ,  
 171 where  $\mathbf{r} = (x, y, z)$ ,  $\psi$  is the wave function and  $E$  is the energy of the states. The LDOS at  
 172  $E_F - 0.2$  eV around the molecule junction of the peanut-shaped dimer is larger than that  
 173 of the dumbbell-shaped dimer. The energetically discrete  $t_{u1}$  orbitals of the  $C_{60}$  molecules  
 174 contributing the electron transport change to the broadened states because of the formation  
 175 of the  $sp^2$ -like connection at the molecule junction. The states in the electrode can easily  
 176 penetrate into the peanut-shaped dimer and the conductance spectrum in Fig. 4 becomes ob-  
 177 scure. Although our computational models do not directly correspond to the tip and surface  
 178 system of STS, the absence of clear peaks of the  $t_{u1}$  orbitals at the center of the polymerized  
 179 cluster in the STS spectrum is related to the smooth behavior of the conductance spectrum  
 180 induced by the  $sp^2$ -like peanut-shaped connections.

#### 181 IV. SUMMARY

182 The atomic configuration of the EB irradiated  $C_{60}$  polymers has been proposed to ex-  
 183 plain the generation of the conductivity in the  $C_{60}$  film through first-principles calculations.  
 184 Although the polymer composed of the [2+2] four-membered rings and dumbbell-shaped  
 185 interlayer connections is a semiconductor with a narrow band gap, the polymer changes to  
 186 exhibit metallic characteristics by forming a peanut-shaped interlayer connection. The cal-  
 187 culations for electron transport for the dumbbell-shaped and peanut-shaped dimers revealed  
 188 that the higher conductance of the peanut-shaped dimer below the Fermi level than that of  
 189 the dumbbell-shaped dimer and the low peak of the conductance spectrum induced by the  
 190  $t_{u1}$  orbitals of the peanut-shaped dimer are relevant to the energetically broadened LDOS at  
 191 the molecule junction caused by the formation of the  $sp^2$ -bonded peanut-shaped connection  
 192 and the metallic property of the EB-irradiated  $C_{60}$  polymer. Rhombohedral film consisting  
 193 of [2+2] four-membered rings, dumbbell-shaped and peanut-shaped connections is a possible  
 194 structure for the metallic  $C_{60}$  polymer observed by STM at the initial stage of EB irradiation.

tion, since the present structure could be formed without significant structural deformation from face-centered cubic  $C_{60}$  bulk and agrees with the rhombohedral structure in the STM image. Although our computational models are limited to the simplified  $C_{60}$  clusters because of the limitation of the computational resources, the large-scale first-principles calculations for the  $C_{60}$  polymers could help to validate the correlation between the STS spectra and the present atomic configuration of the polymers and will be carried out in a future.

## ACKNOWLEDGEMENTS

The authors would like to thank Kikuji Hirose and Yoshitada Morikawa of Osaka University for fruitful discussion. This research was partially supported by Strategic Japanese-German Cooperative Program from Japan Science and Technology Agency and Deutsche Forschungsgemeinschaft, by a Grant-in-Aid for Scientific Research on Innovative Areas (Grant No. 22104007) from the Ministry of Education, Culture, Sports, Science and Technology, Japan. The numerical calculation was carried out using the computer facilities of the Institute for Solid State Physics at the University of Tokyo, the Research Center for Computational Science at the National Institute of Natural Science, Center for Computational Sciences at University of Tsukuba, and the Information Synergy Center at Tohoku University.

---

<sup>1</sup> *Fullerene Polymers and Fullerene Polymer Composites*, edited by P.C. Eklund and A.M. Rao (Springer, Berlin, 2000) and references therein.

<sup>2</sup> S. Okada and A. Oshiyama, *Phys. Rev. B* **68**, 235402 (2003).

<sup>3</sup> J. Onoe, T. Nakayama, M. Aono, and T. Hara, *Appl. Phys. Lett.* **82**, 595 (2003).

<sup>4</sup> See, e.g., J. Onoe, A. Takashima, and Y. Toda, *Appl. Phys. Lett.* **97**, 241911 (2010).

<sup>5</sup> S. Ueda, K. Ohno, Y. Noguchi, S. Ishii, and J. Onoe, *J. Phys. Chem. B* **110**, 22374 (2006).

<sup>6</sup> J. Onoe, T. Ito, S.I. Kimura, K. Ohno, Y. Noguchi, and S. Ueda, *Phys. Rev. B* **75**, 233410 (2007).

<sup>7</sup> M. Nakaya, M. Aono, and T. Nakayama, *Carbon* **49**, 1829 (2011).

<sup>8</sup> P. Hohenberg and W. Kohn, *Phys. Rev.* **136**, B864 (1964).



- 222 <sup>9</sup> K. Hirose, T. Ono, Y. Fujimoto, and S. Tsukamoto, *First Principles Calculations in Real-Space*  
223 *Formalism, Electronic Configurations and Transport Properties of Nanostructures* (Imperial  
224 College, London, 2005).
- 225 <sup>10</sup> T. Ono and K. Hirose, Phys. Rev. Lett. **82**, 5016 (1999); Phys. Rev. B **72**, 085115 (2005); T.  
226 Ono, M. Heide, N. Atodiresei, P. Baumeister, S. Tsukamoto, and S. Blügel, Phys. Rev. B **82**,  
227 205115 (2010).
- 228 <sup>11</sup> We used the norm-conserving pseudopotentials NCPS97 constructed by K. Kobayashi. See K.  
229 Kobayashi, Comput. Mater. Sci. **14**, 72 (1999).
- 230 <sup>12</sup> N. Troullier and J. L. Martins, Phys. Rev. B **43**, 1993 (1991).
- 231 <sup>13</sup> J. P. Perdew and A. Zunger, Phys. Rev. B **23**, 5048 (1981).
- 232 <sup>14</sup> X. Chen, S. Yamanaka, K. Sako, Y. Inoue, and M. Yasukawa, Chem. Phys. Lett. **356**, 291  
233 (2002).
- 234 <sup>15</sup> S. Tsukamoto and T. Nakayama, J. Chem. Phys. **122**, 074702 (2005).
- 235 <sup>16</sup> M. Núñez-Regueiro, L. Marques, J.-L. Hodeau, O. Béthoux, and M. Perroux, Phys. Rev. Lett.  
236 **74**, 278 (1995).
- 237 <sup>17</sup> J. Tersoff and D.R. Hamann, Phys. Rev. B **31**, 805 (1985).
- 238 <sup>18</sup> H. Hövel, B. Grimm, M. Bödecker, K. Fieger, and B. Reihl, Surf. Sci. **463**, L603 (2000); H.  
239 Hövel and I. Barke, Prog. Surf. Sci. **81**, 53 (2006); M. De Menech, U. Saalman, and M.E.  
240 Garcia, New J. Phys. **9**, 340 (2007).
- 241 <sup>19</sup> M. Otani, T. Ono, and K. Hirose, Phys. Rev. B **69**, 121408(R) (2004).
- 242 <sup>20</sup> T. Ono and K. Hirose, Phys. Rev. Lett. **98**, 026804 (2007).
- 243 <sup>21</sup> G. Schull, T. Frederiksen, M. Brandbyge, and R. Berndt, Phys. Rev. Lett. **103**, 206803 (2009).
- 244 <sup>22</sup> H. Nakayama, T. Ono, H. Goto, and K. Hirose, Sci. Tech. Adv. Mater. **8**, 196 (2007).
- 245 <sup>23</sup> L.-L. Wang and H.-P. Cheng, Phys. Rev. B **69**, 165417 (2004).
- 246 <sup>24</sup> Y. Fujimoto and K. Hirose, Phys. Rev. B **67**, 195315 (2003).
- 247 <sup>25</sup> L. Kong, M.L. Tiago, and J.R. Chelikowsky, Phys. Rev. B **73**, 195118 (2006).
- 248 <sup>26</sup> Y. Egami, K. Hirose, and T. Ono, Phys. Rev. E **82**, 056706 (2010).
- 249 <sup>27</sup> L. Kong, J.R. Chelikowsky, J.B. Neaton, and S.G. Louie, Phys. Rev. B **76**, 235422 (2007).
- 250 <sup>28</sup> M. Büttiker, Y. Imry, R. Landauer, and S. Pinhas, Phys. Rev. B **31**, 6207 (1985).

251 **FIGURES**

252

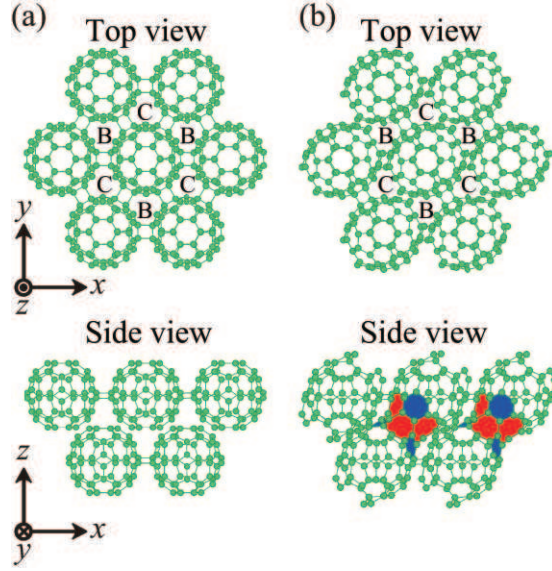


FIG. 1. (color online) Geometric structure of 3D  $C_{60}$  polymer phases. (a) Polymer bonded by only [2+2] four-membered rings and dumbbell-shaped connections and (b) polymer in which one of three dumbbell-shaped connections deforms to the peanut-shaped connection. The shaded segments in (b) represent the hexagons (blue) and heptagons (red) of the peanut-shaped connection. B and C in the top views correspond to the positions of  $C_{60}$  molecules in the upper and lower layers.

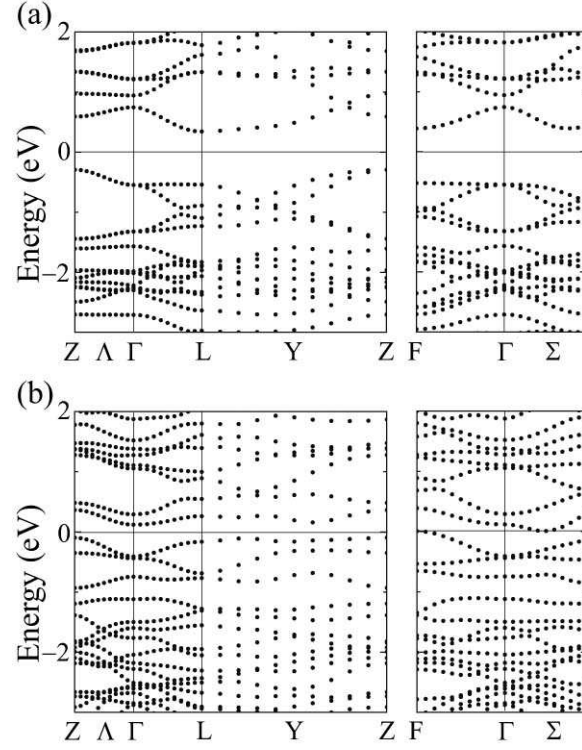


FIG. 2. Band structures of 3D  $C_{60}$  polymers of models (a) and (b) in Fig. 1. Zero energy was chosen as the Fermi level.

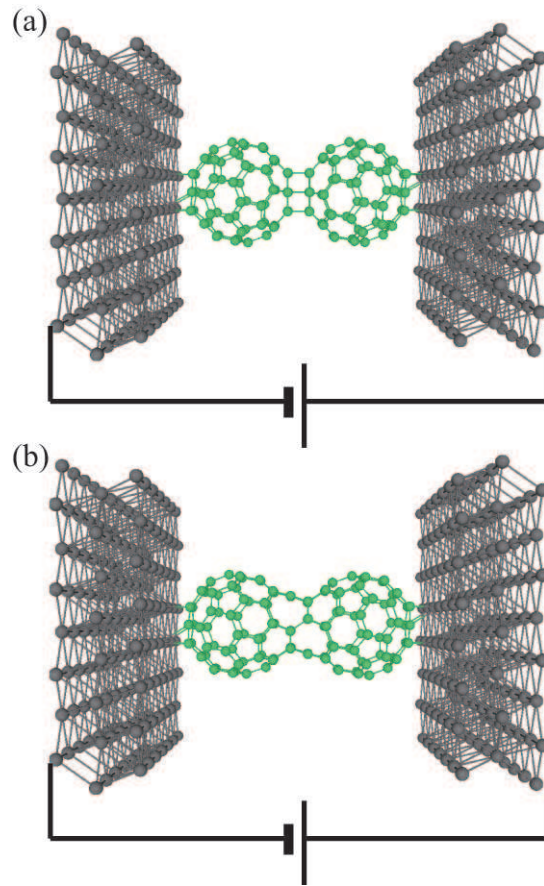


FIG. 3. (color online) Computational model where C<sub>60</sub> dimer is suspended between Al(111) electrodes. (a) Dumbbell-shaped dimer and (b) peanut-shaped dimer.

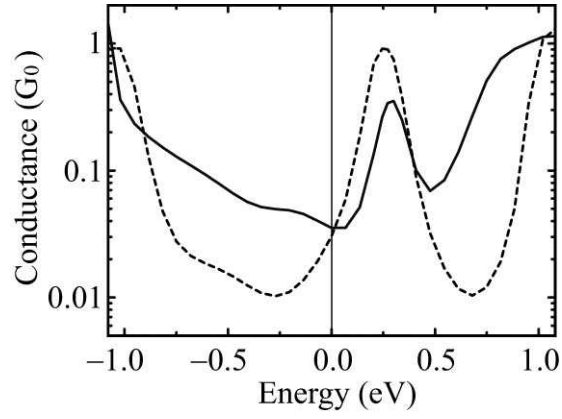


FIG. 4. Conductance spectra as function of energy of incident electrons. The dashed curve represents the conductance of the dumbbell-shaped dimer and the solid curve that of the peanut-shaped dimer. Zero energy was chosen as the Fermi level.

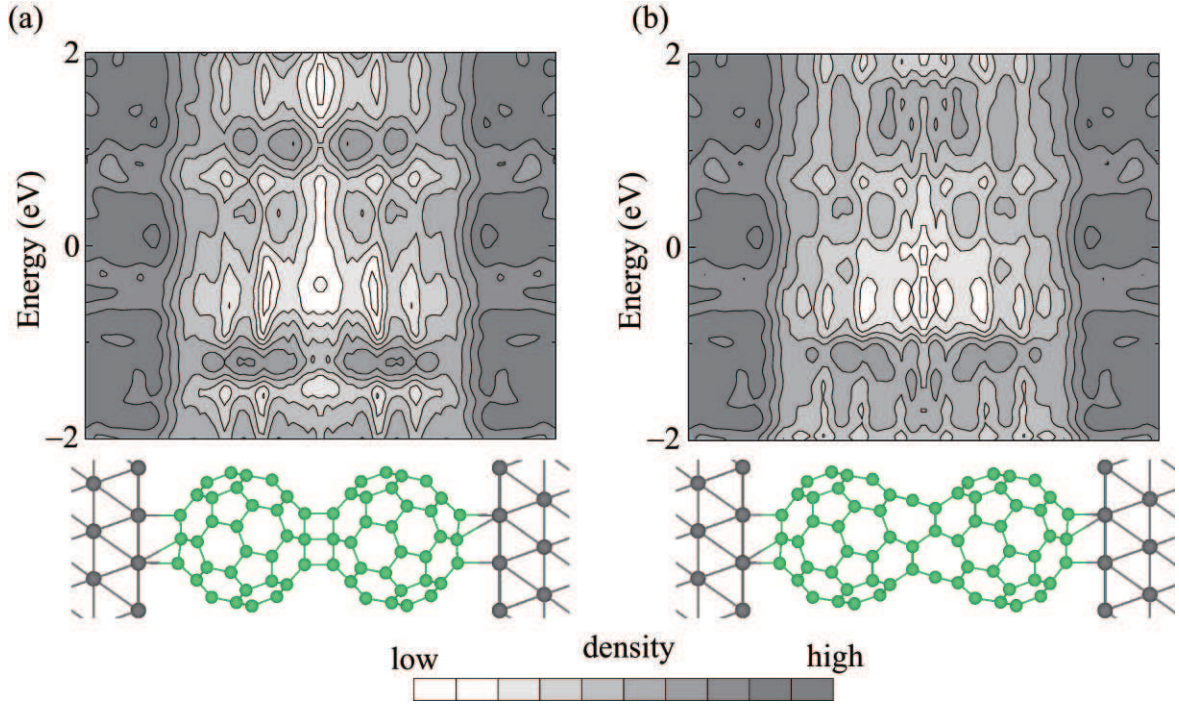


FIG. 5. (color online) Distributions of LDOS integrated on plane parallel to dimer as functions of relative energy from Fermi level. Zero energy is chosen as the Fermi level. Each contour represents twice or half the density of the adjacent contour lines, and the lowest contour is  $2.56 \times 10^{-4} e/eV/\text{bohr}$ . The atomic configurations below the graph are visual guides.